2-2005

Transient response of ARROW VCSELs

Chyng Wen TEE
Singapore Management University, cwtee@smu.edu.sg

S. F. Yu

R. V. Penty

I. H. White

DOI: https://doi.org/10.1109/JQE.2004.839713

Published in IEEE Journal of Quantum Electronics, 2005 February, Volume 41, Issue 2, Pages 140-147
https://doi.org/10.1109/JQE.2004.839713

Transient Response of ARROW VCSELs

C. W. Tee, *Student Member, IEEE*, S. F. Yu, *Senior Member, IEEE*, R. V. Penty, *Member, IEEE*, and I. H. White, *Senior Member, IEEE*

***Abstract*—The transient response of antiresonant reflecting optical waveguide (ARROW) vertical-cavity surface-emitting lasers (VCSELs) is analyzed. It is found that under current modulation, the radiation loss of the transverse-leaky mode decreases during the $\langle \mathrm{ON} \rangle$ state of the lasers but increases during the $\langle \mathrm{OFF} \rangle$ state. Numerical analysis shows that this variation in radiation loss is due to the carrier-induced refractive-index depression that arises from spatial-hole-burning of carrier concentration. It is noted that the increment in radiation loss during the $\langle \mathrm{OFF} \rangle$ state can be used to prevent net modal gain of the transverse-leaky mode from reacquiring threshold after turn-off. Hence, a new method to design ARROW, based on the variation in radiation loss, is proposed to eliminate the excitation of secondary pulsation in VCSELs. The influence of thermal lensing effects on the excitation of secondary pulsation during the $\langle \mathrm{OFF} \rangle$ state of the lasers is also investigated.**

***Index Terms*—Antiresonant reflecting optical waveguide (ARROW), radiation loss, secondary pulsation, semiconductor laser modeling, spatial hole burning, turn-off transients, vertical-cavity surface-emitting lasers (VCSELs) .**

I. Introduction

SECONDARY pulsation during the turn-off transient in vertical-cavity surface-emitting lasers (VCSELs) poses a limit on the maximum attainable bit rate and minimum bit-error-rate in optical communication systems [1]–[4]. Numerical analysis has shown that for VCSELs under current modulation, excitation of secondary pulsation is due to the joint effects of spatial hole burning (SHB) and diffusion of carrier concentration. This is because during the $\langle \mathrm{ON} \rangle$ state of the VCSEL, thr SHB of carrier concentration due to stimulated recombination causes a large spatial gradient of carrier concentration. Once the laser is switched to the $\langle \mathrm{OFF} \rangle$ state, the corresponding diffusion of carrier concentration will refill the spatial-hole, which enables lasing modes to make a transient recovery (i.e., excitation of secondary pulsation) after turn-off.

In order to suppress secondary pulsation, it has been proposed to construct a large-aperture VCSEL with strong current confinement so that the spatial gradient of carrier concentration can be minimized [1]. In addition, modulating multimode VCSELs with a high turn-on current can also ensure a large power ratio between $\langle \mathrm{ON} \rangle$ state and peak power of secondary pulses, thus minimizing the influence of secondary pulsation [2]. However, these suggestions are not ideal for practical application of VCSELs. This is because the most common way to achieve current confinement in large-aperture VCSELs is by means of ion implantation (i.e., weak current confinement). In addition, multimode operation in VCSELs will also deteriorate the high-speed performance of optical communication systems. Hence, a novel design of VCSELs with weak current confinement that has the capability to eliminate secondary pulsation while maintaining high-power single-mode operation is highly desired.

Recently, cylindrical antiresonant reflecting optical waveguide (ARROW) has been employed to achieve high-power single-mode emission in VCSELs [5]. Unlike conventional index- or gain- guided VCSELs, the ARROW device supports transverse-leaky modes. In addition, the transverse-leaky mode has a radiation loss that is determined by the antiresonant condition of the ARROW. Under current modulation, the antiresonant condition of the transverse-leaky mode will be altered due to the variation in carrier-induced refractive-index depression [6]. In fact, this bias-dependent behavior of the transverse-leaky mode (i.e., radiation losses) can be used to suppress the excitation of secondary pulsation. If the radiation loss of the transverse-leaky mode can be increased sufficiently during $\langle \mathrm{OFF} \rangle$ state of the lasers, the net modal gain of the leaky modes will not be able to achieve transient recovery. In order to achieve suppression of secondary pulsation, it is necessary to study the transient response of ARROW VCSELs. In this paper, the transient response of ARROW VCSELs under current modulation is investigated. Secondary pulsation in ARROW VCSELs under multi- and single-transverse-leaky mode operations is analyzed, and a new design approach to eliminate secondary pulsation is also proposed. In addition, the influence of thermal lensing effects on the excitation of secondary pulsation is investigated.

II. Theoretical Model

Fig. 1 shows the schematic of an ARROW VCSEL. It is assumed that the ARROW has a low-index core region with diameter d_1 ($=12\ \mu$m), which is surrounded by two cladding layers with thickness s (first cladding layer) and d_2 (second cladding layer). The refractive indices of the core (n_1), first (n_2), second (n_3), and the outer cladding layers (n_4) are 3.3, 3.35, 3.3, and 3.35, respectively. The free-space lasing wavelength is assumed to be 0.98 μm. Due to large modal discrimination in ARROW, only two leaky modes (i.e., LM_{01} and LM_{11}, where LM denotes leaky modes) that have the lowest radiation losses are considered in the following analysis.

The photon rate equations that describe the competition of the transverse-leaky mode inside the ARROW VCSEL can be written as [7]

$$\frac{dS_m}{dt} = \nu_g(\Gamma_z\langle g_m\rangle - \alpha_m - \zeta_m)S_m + \beta_{\mathrm{sp}}\Gamma_z B_{\mathrm{sp}}\langle N\rangle^2 \quad (1)$$

Manuscript received May 27, 2004; revised September 10, 2004. The work of C. W. Tee is supported by Cambridge Commonwealth Trust.

C. W. Tee, R. V. Penty, and I. H. White are with the Center for Photonic Systems, Cambridge University Engineering Department, Cambridge CB3 0FD, U.K. (e-mail: cwt23@cam.ac.uk).

S. F. Yu is with the School of Electrical and Electronic Engineering, Nanyang Technological University, Singapore 639798.

Digital Object Identifier 10.1109/JQE.2004.839713

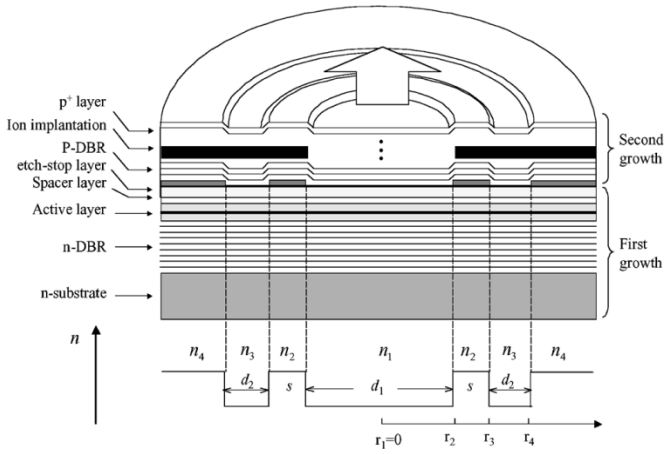

Fig. 1. Schematic of an ARROW VCSEL.

where the subscript m ($=01(\mathrm{LM}_{01})$ or $=11(\mathrm{LM}_{11})$) is used to label the order of the transverse-leaky mode. S_m is the photon density, $\Gamma_z(=0.06)$ is the confinement factor along the longitudinal direction, ν_g ($=8.33\times10^9$ cm/s) is the group velocity, B_{sp} ($=1\times10^{-10}$ cm^3/s) is the bimolecular recombination coefficient, and $\beta_s(=1\times10^{-5})$ is the spontaneous emission factor. α_m and ζ_m (50 cm^{-1} for LM_{01} and 65 cm^{-1} for LM_{11}) are the radiation and modal absorption losses of the transverse-leaky mode. The spatial average of modal gain $\langle g_m\rangle$ is given by

$$\langle g_m\rangle = \int_0^\infty g(N)|\psi_m(r,t)|^2 r\,dr \Big/ \int_0^\infty |\psi_m(r,t)|^2 r\,dr \quad (2)$$

where r is the transverse direction, $g(N) = a_N\log(N(r,t)/N_t), N$ is the carrier concentration, N_t ($=1.5\times10^{18}$ cm^{-3}) is the transparent carrier density, and a_N ($=1.5\times10^3$ cm^{-1}) is the gain coefficient. $\langle N\rangle$ has the similar definition as $\langle g_m\rangle$. In (2), the wave function, ψ_m, which describes the transverse field profile within ARROW VCSELs, is given by [8]

$$\psi_m(r,t) = E^+H_m^{(1)}(\beta_m(t)r) + E^-H_m^{(2)}(\beta_m(t)r) \quad (3)$$

where $E^+(E^-)$ is the positive (negative) traveling field amplitude along the transverse direction, $H_m^{(1)}(H_m^{(2)})$ is the mth-order Hankel function of the first (second) kind, and $\beta_m(t)$ is the propagation constant of the transverse-leaky mode. A field-transfer matrix model for cylindrical waveguide structure is used to evaluate $\beta_m(t)$ in (3) by solving the appropriate eigenequation [8]. It should be noted that since $\beta_m(t)$ is time-varying due to the influence of current modulation, the radiation loss, defined as $\alpha(t) = 2*\mathrm{Im}\{\beta_m(t)\}/k_0$, is also a function of time. The method to determine $\beta_m(t)$ is presented in the Appendix.

The rate equation of carrier concentration N can be written as

$$\frac{\partial N}{\partial t} = D\left[\frac{1}{r}\frac{\partial N}{\partial r} + \frac{\partial^2 N}{\partial r^2}\right] + \frac{J(r,t)}{qd} - \frac{N}{\tau_N} - v_g\sum g(N)|\psi_m|^2 S_m \quad (4)$$

where D ($=5$ cm^2/s) is the diffusion coefficient, q ($=1.602\times10^{-19}$ C) is the electron charge, d ($=0.1\times10^{-4}$ cm) is the thickness of active layer, and τ_N ($=1$ ns) is the carrier lifetime. The injection current J from a circular disk metal electrode can be written as [9]

$$J(r,t) = \begin{cases} J_e(t), & r \le d_1/2 \\ J_e(t)\exp(-(r-d_1)/2)/r_o), & r > d_1/2 \end{cases} \quad (5)$$

where $J_e(t)$ denotes the current density at the edge and within the contact area ($r \le d_1/2$), r_o ($=1$ μm) is the effective diffusion length (i.e., weak current confinement). The variation of the refractive index Δn due to the change in carrier concentration ΔN is given by

$$\Delta n = -\alpha_H\frac{\lambda}{4\pi}\Gamma_z\frac{a_N}{N}\Delta N \quad (6)$$

where $\alpha_H(=6)$ is the linewidth enhancement factor and λ ($=0.98$ μm) is the free-space wavelength.

Temperature rise along the transverse direction of the active layer ΔT_r can be calculated by solving the heat conduction equation using Green's function method. The numerical technique used to determine ΔT_r can be found in [7]. The heat-induced index change (i.e., thermal lensing effects) can be expressed as

$$\Delta n_T = \frac{\partial n}{\partial T}\Delta T_r \quad (7)$$

where $\partial n/\partial T(\sim 1.5\times10^{-4})$ is the heat-induced index-change coefficient.

III. Numerical Analysis

In this section, the turn-off transients of ARROW VCSELs under multi- and single-transverse-leaky mode operations are studied. Design methodology of ARROW structure to suppress secondary pulsation in VCSELs is elaborated, and the fabrication tolerance of the proposed design is investigated subsequently. Initial studies have neglected the influence of thermal lensing effects in order to isolate and quantify the role of SHB of carrier concentration on the behavior of radiation loss and secondary pulsation. Finally, the influence of thermal lensing effects on the transient response of the lasers is studied and compared with previous cold-cavity analysis.

A. Multitransverse-Leaky-Mode Operation

Multitransverse-leaky-mode operation can be supported in ARROW VCSELs if the dimension of ARROW is selected such that the radiation losses of several leaky modes are relatively low. Fig. 2 plots the radiation losses of four lowest loss leaky modes ($\mathrm{LM}_{01}, \mathrm{LM}_{11}, \mathrm{LM}_{02}, \mathrm{LM}_{12}$) versus d_2. The value of s had been set to 1.28 μm to satisfy the antiresonant condition of LM_{01} [9]. It is observed that at the point where $d_2 = 2.6$ μm, the radiation loss of LM_{11} is close to that of LM_{01}. Therefore, ARROW VCSELs with $s = 1.28$ μm and $d_2 = 2.6$ μm is expected to support multitransverse-leaky mode operation (both LM_{01} and LM_{11}). The corresponding field-intensity profiles of LM_{01} and LM_{11} are also shown in the inset of Fig. 2.

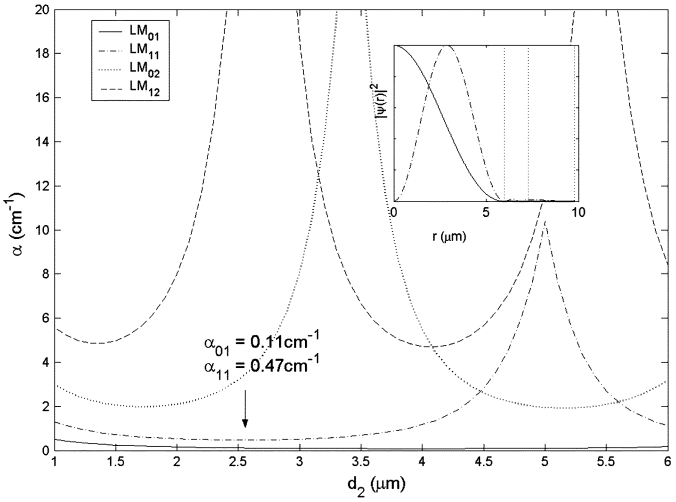

Fig. 2. Radiation loss of LM_{01}, LM_{11}, LM_{02}, and LM_{12} with $d_2 = 2.6\,\mu$m. Inset shows the field-intensity profile of LM_{01} and LM_{11}.

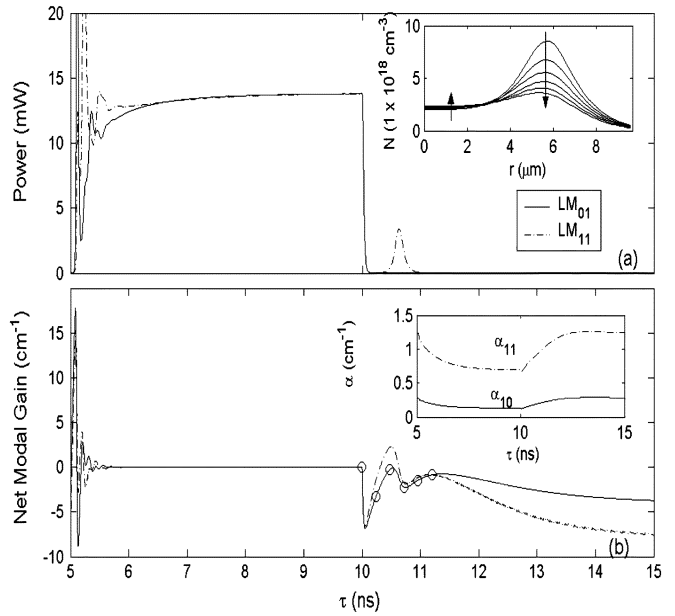

Fig. 3. (a) Dynamical evolution of output power in multitransverse leaky mode operation of ARROW VCSEL. Carrier concentration profiles during turn-off transients are plotted in the inset at a time interval of 0.25 ns, as indicated by circles in (b). (b) Dynamical evolution of net modal gain. The radiation losses of the transverse leaky modes are plotted in the inset.

The laser with the above design is initially biased at $\langle\mathrm{OFF}\rangle$ state by a current density of $J_{\mathrm{off}} = 0.9J_{\mathrm{th}}$ for 5 ns, where J_{th} is the threshold current density. A squarewave modulation current with a period of 5 ns and magnitude of $\langle\mathrm{ON}\rangle$ ($\langle\mathrm{OFF}\rangle$) state current density $J_{\mathrm{on}} = 4.5J_{\mathrm{th}}(J_{\mathrm{off}} = 0.9J_{\mathrm{th}})$ is then applied to the laser. Fig. 3 shows the corresponding transient response of the output power and net modal gain. It is observed that only LM_{11} exhibits secondary pulsation with a peak power of $\sim$4 mW during $\langle\mathrm{OFF}\rangle$ state. This is different from small aperture VCSELs, where secondary pulsation only occurs on the fundamental transverse mode [2]. This behavior can be understood by comparing the carrier diffusion length, $L_D(=\sqrt{D\tau_N})$, and aperture size d_1 of the VCSELs. Recall that excitation of secondary pulsation during the turn-off transient is due to carrier diffusion that refills the SHB of carrier concentration, enabling lasing to make a transient recovery in the $\langle\mathrm{OFF}\rangle$ state. If $d_1 \gg L_D$, carriers can only diffuse a short distance to refill a portion of the spatial hole close to the region of high carrier concentration. Hence, secondary pulsation will occur in LM_{11} due to large spatial overlapping area between the profiles of LM_{11} and carrier concentration. This explains our observation in Fig. 3, where we have $d_1 = 12\,\mu$m and $L_D = 0.7\,\mu$m. On the other hand, if the magnitude of d_1 and L_D are of the same order (e.g., $d_1 = 6\,\mu$m and $L_D = 1.4\,\mu$m, as in [2]), carrier diffusion can easily refill the SHB of carrier concentration. Consequently, transverse mode with maximum spatial overlap with profile of carrier concentration (i.e., LM_{01}) will exhibit secondary pulsation [2].

It is noted that the radiation losses of LM_{01} and LM_{11} vary during $\langle\mathrm{ON}\rangle$ and $\langle\mathrm{OFF}\rangle$ states of the laser [inset of Fig. 3(b)]. This behavior of ARROW VCSELs can be understood by studying the carrier-induced refractive-index depression inside the ARROW. Initially, the dimension of ARROW is selected such that both LM_{01} and LM_{11} satisfy the antiresonant conditions (lowest radiation losses). However, injection of modulation current causes depression of refractive index within the core region, hence affecting the optical thickness of the ARROW. During $\langle\mathrm{OFF}\rangle$ state, the build-up of carrier concentration causes both LM_{01} and LM_{11} to shift away from their antiresonant conditions. This causes the corresponding radiation losses to increase. When the laser is switched to $\langle\mathrm{ON}\rangle$ state, stimulated emission causes depletion of carrier concentration. The magnitude of carrier-induced refractive-index depression is therefore smaller, causing the corresponding radiation losses to decrease. Furthermore, as the magnitude of the radiation losses of the two transverse-leaky modes is small, the variation in radiation loss during $\langle\mathrm{ON}\rangle$ and $\langle\mathrm{OFF}\rangle$ state is also relatively small.

B. Single Transverse-Leaky-Mode Operation

The situation changes if the laser is designed to support only single-mode emission. This can be achieved by selecting the dimension of ARROW to obtain maximum radiation loss margin (difference in radiation losses between LM_{01} and LM_{11}). Fig. 4 plots the radiation losses of the four leaky modes versus s. The length of d_2 is set to 3.9 μm so that the radiation loss of LM_{01} is minimized (refer to Fig. 2). It is noted that when $s = 2.46\,\mu$m, the radiation loss margin between LM_{01} and the other higher order leaky modes is maximized. Therefore, it is expected that the ARROW is capable of sustaining single-mode emission if s is set to 2.46 μm.

Fig. 5 plots the turn-off transients of the above single-mode ARROW VCSEL. It is observed that LM_{01} exhibits secondary pulsation during $\langle\mathrm{OFF}\rangle$ state. This shows that large aperture devices with weak current confinement are not immune to secondary pulsation. Furthermore, it is observed that the transient response of α_{01} is similar to that given in Fig. 3. The variation in the radiation loss during $\langle\mathrm{ON}\rangle$ and $\langle\mathrm{OFF}\rangle$ state is larger compared to multimode operation. However, the magnitude of this variation in radiation loss is not large enough to suppress secondary pulsation.

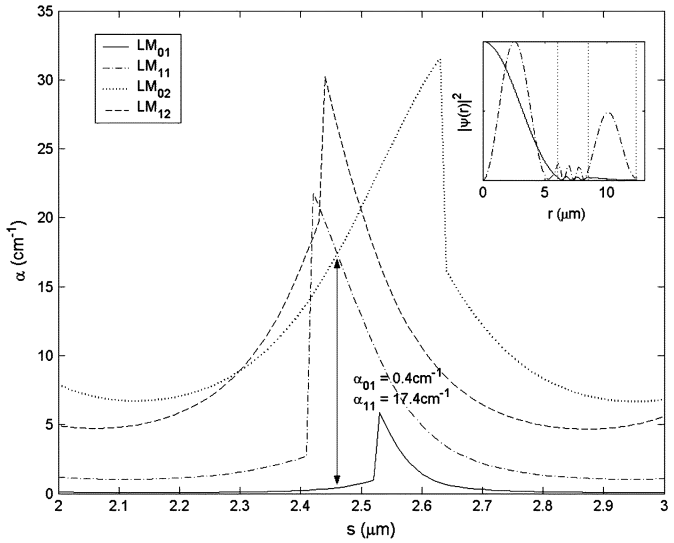

Fig. 4. Radiation loss of $\mathrm{LM}_{01}, \mathrm{LM}_{11}, \mathrm{LM}_{02}$, and LM_{12} with $s = 2.46\ \mu$m. Inset shows the field-intensity profile of LM_{01} and LM_{11}.

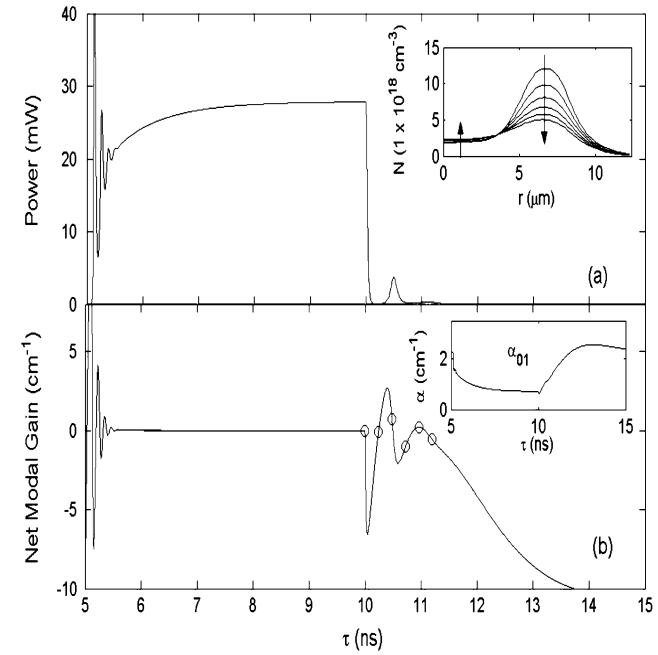

Fig. 5. Dynamical evolution of (a) output power and (b) net modal gain of ARROW VCSEL designed for single mode emission. The carrier concentration profiles during turn-off transients and radiation loss of the transverse leaky mode are plotted in the inset of (a) and (b), respectively.

C. Novel Design of ARROW: Suppression of Secondary Pulsation in VCSELs

From the above analysis, it is shown that current modulation causes variation in radiation loss of the leaky modes. Increment in radiation loss also reduces transverse mode confinement, leading to a lower net modal gain. It is noted that this effect can be used to suppress secondary pulsation during turn-off transient by decreasing the net modal gain in the $\langle \mathrm{OFF} \rangle$ state of the lasers. However, the increment in radiation loss (as shown in Figs. 3 and 5) is smaller than the increment in net modal gain of the leaky modes during $\langle \mathrm{OFF} \rangle$ state. In order to suppress

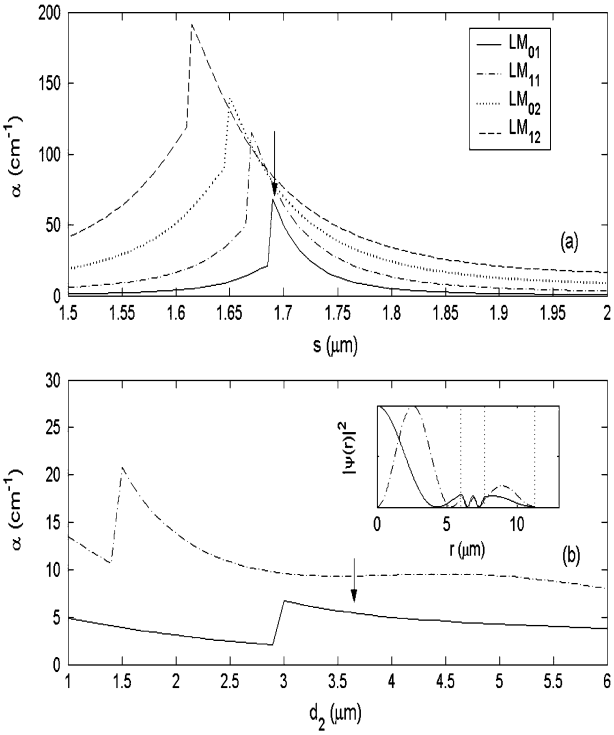

Fig. 6. Radiation loss of $\mathrm{LM}_{01}, \mathrm{LM}_{11}, \mathrm{LM}_{02}, \mathrm{LM}_{12}$ in (a) S-ARROW and (b) ARROW with $s = 1.69\ \mu$m. Inset shows the field-intensity profile of LM_{01} and LM_{11}.

secondary pulsation, it is necessary to increase the magnitude of this variation in radiation loss to more than 6 cm^{-1} during $\langle \mathrm{OFF} \rangle$ state. One possible way to increase the variation in radiation loss is to select the dimension of ARROW close to the resonance condition. In this case, the variation in optical thickness of the ARROW will result in a large variation of radiation loss (e.g., see Figs. 2 and 4, the curves have very shape peaks at the resonance conditions [10]), such that the increment in radiation loss during the $\langle \mathrm{OFF} \rangle$ state is sufficient to prevent the net modal gain of the leaky modes from reacquiring threshold after turn-off.

In order to operate near resonant condition, the value of s is selected where the radiation loss of LM_{01} is the maximum [see Fig. 6(a)]. This corresponds to $s \sim 1.69\ \mu$m, where a radiation loss of $\alpha_{01} \sim 64\ \mathrm{cm}^{-1}$ is obtained. Clearly, this α_{01} value is too large for practical application, so the value of d_2 is varied to reduce α_{01} to an acceptable value [see Fig. 6(b)]. It is noted that for $d_2 \sim 3.6\ \mu$m, the radiation loss, α_{01}, is reduced to $\sim 6\ \mathrm{cm}^{-1}$ (but still close to resonance), and the radiation loss margin between LM_{01} and the next higher order mode is maintained at a relatively large value ($\sim 5\ \mathrm{cm}^{-1}$). The field-intensity profiles of LM_{01} and LM_{11} of the proposed design are also shown in the inset of Fig. 6(b).

Fig. 7 shows the transient response of ARROW VCSELs with $s = 1.69\ \mu$m and $d_2 = 3.6\ \mu$m. It is observed that during $\langle \mathrm{ON} \rangle$ state, the radiation loss of LM_{01} is $\sim 5\ \mathrm{cm}^{-1}$. After turn-off, the radiation loss experiences a steep increment (from ~ 5 to $\sim 12\ \mathrm{cm}^{-1}$) within 0.5 ns. Note that although the net modal gain of LM_{01} undergoes a bounce right after turn-off, the subsequent large increment in radiation loss significantly suppresses

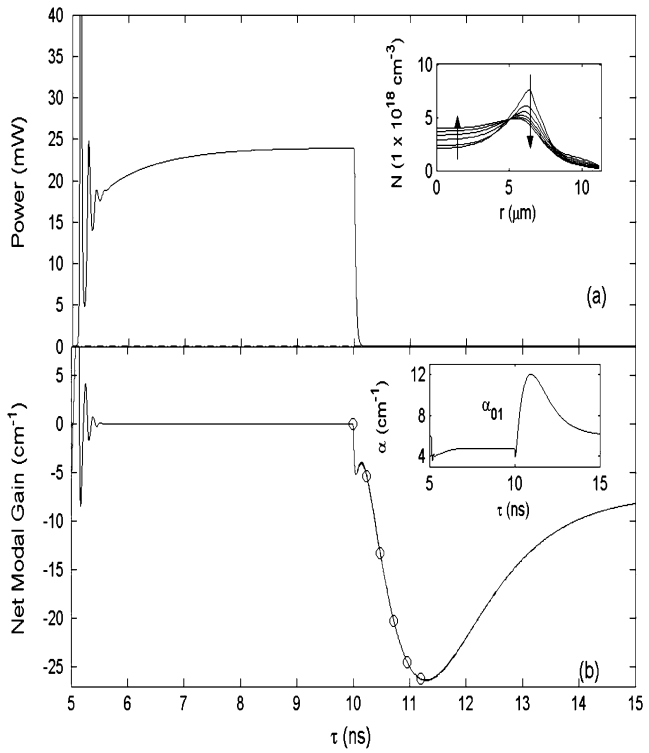

Fig. 7. Dynamical evolution of (a) output power and (b) net modal gain of ARROW VCSEL designed for suppression of secondary pulse. The carrier concentration profiles during turn-off transients and radiation loss of the transverse leaky mode are plotted in the inset of (a) and (b), respectively.

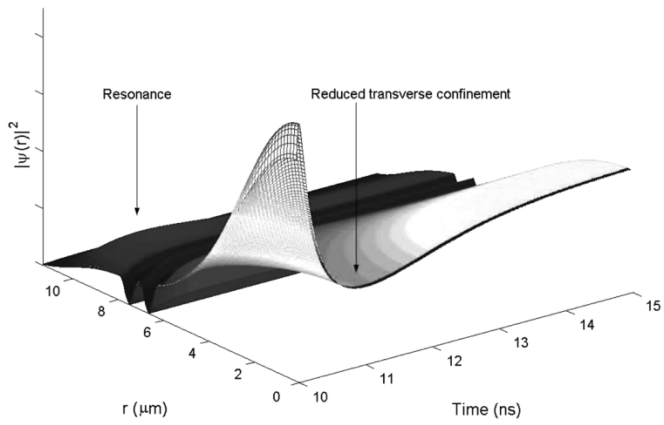

Fig. 8. Field-intensity profile of LM_{01} during $\langle \mathrm{OFF} \rangle$ state of the laser.

the net modal gain and prevent it from reacquiring threshold. From the figure, it is noted that although the radiation loss increase significantly right after turn-off, it will eventually reduce to $\sim 6\ \mathrm{cm}^{-1}$. This mechanism can be explained by the transient response of the field-intensity profile of LM_{01} during $\langle \mathrm{OFF} \rangle$ state, as shown in Fig. 8. It is noted that initially when the laser enters $\langle \mathrm{OFF} \rangle$ state, the field-intensity profile shifted toward the second cladding layer, showing that the operation point is moving toward resonance. However, the field-intensity profile will gradually move back into the core region, and the radiation loss will be reduced to a reasonably small value.

The preceding studies have established the fact that carrier induced index change is the primary effect that leads to the

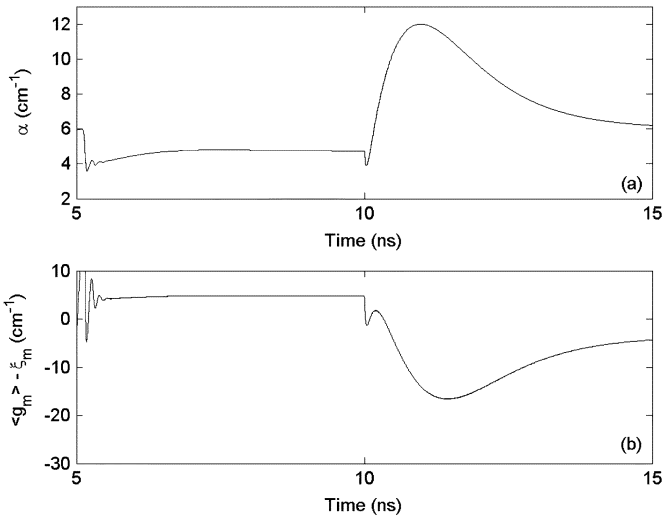

Fig. 9. Transient response of (a) radiation loss, α, and (b) weighted-modal-gain, $\langle g_m \rangle - \zeta_m$.

suppression of secondary pulsation. This is obtained by preventing the net modal gain, defined as $\langle g_m \rangle - \zeta_m - \alpha$, from reacquiring threshold after turn-off. In order to clarify the dependence of $\langle g_m \rangle - \zeta_m$ and radiation loss on the suppression of secondary pulsation, Fig. 9 plots the transient response of their individual contribution to the net modal gain. It is observed that $\langle g_m \rangle - \zeta_m$ is clamped to its threshold value during the $\langle \mathrm{ON} \rangle$ state ($\sim 4.75\ \mathrm{cm}^{-1}$), and does not exceed threshold during the turn-off transient. Therefore, it is clear that the decrement in modal gain due to the reduction of modal confinement is the dominant effect in the suppression of secondary pulsation. However, it must be mentioned that while radiation loss variation does not have a direct impact, its correlation with the modal confinement of the waveguide provides an efficient way of designing structure capable of suppressing secondary pulsation.

D. Fabrication Tolerance of the ARROW

The threshold current density J_{th} of ARROW VCSELs can be deduced analytically from (1) and (4) if the nonuniform distribution of carrier concentration is ignored. It can be shown that J_{th} can be expressed as

$$J_{\mathrm{th}} \approx \frac{qdN_t}{\tau_N} \exp\left(\frac{\alpha_m + \zeta_m}{\Gamma_z a_N}\right). \tag{8}$$

In addition, influence of radiation loss on the differential quantum efficiency η_d can be expressed as

$$\eta_d \approx \frac{\zeta_m}{\alpha_m + \zeta_m}. \tag{9}$$

According to the design approach proposed in Section III-C, α_{01} has to be increased from 0.1 to 6 cm^{-1}, which implies that there will also be a corresponding increment (decrement) of $J_{\mathrm{th}}(\eta_d)$. From (8), it can be shown that the increment of J_{th} is not more than 10%. Furthermore, the reduction of η_d obtained from (9) is less than 10%. Our numerical simulation has verified that the variation of η_d is less than 20% during some extreme

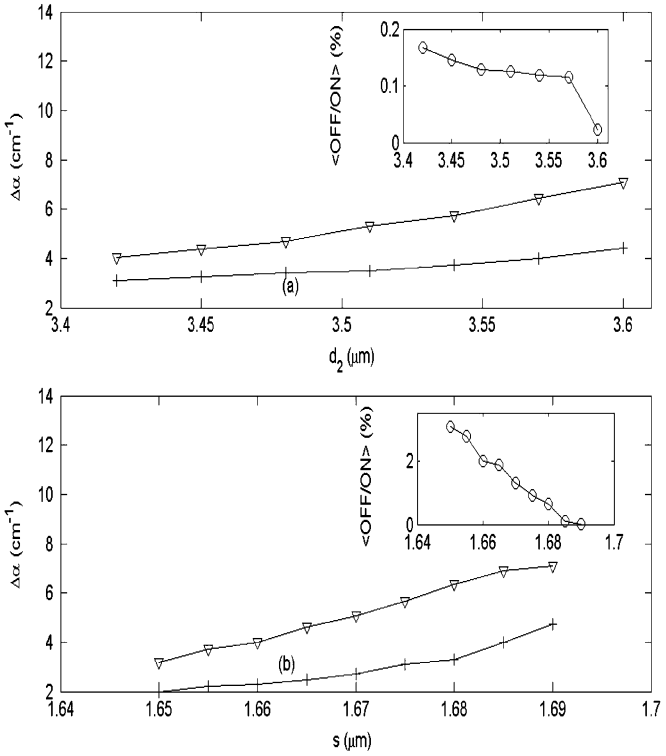

Fig. 10. Influence of (a) second cladding layer thickness, d_2, and (b) first cladding layer thickness, s, on the radiation loss during $\langle \mathrm{OFF} \rangle$ state ($+$), and the peak variation in radiation loss (∇). Inset shows the corresponding $\langle \mathrm{OFF/ON} \rangle$ ratio.

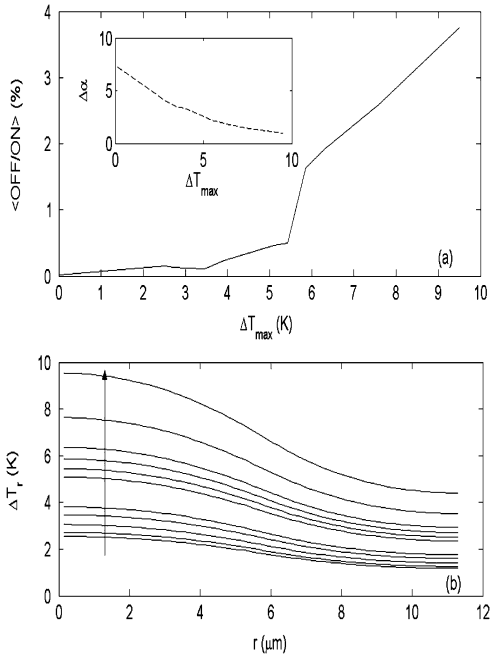

Fig. 11. (a) $\langle \mathrm{OFF/ON} \rangle$ ratio of the proposed structure plotted against maximum temperature rise. Inset shows the radiation loss variation. (b) Temperature rise along the transverse direction.

conditions. Hence, this implies that the design proposed in Section III-C would not significantly deteriorate the performance of VCSELs since the changes in J_{th} and η_d are small.

Due to uncertainty in the fabrication process of ARROW VCSELs, the actual values of s and d_2 may vary. Therefore, it is necessary to investigate the tolerance of the design (i.e., the allowed variation of s and d_2) for effective suppression of secondary pulsation. Fig. 10 plots the radiation loss during $\langle \mathrm{OFF} \rangle$ state as well as the variation in radiation loss against Fig. 10(a) d_2 and Fig. 10(b) s under current modulation. The inset in Fig. 10(a)–(b) plots the $\langle \mathrm{OFF/ON} \rangle$ ratio versus $d_2(s)$. The $\langle \mathrm{OFF/ON} \rangle$ ratio is defined as the ratio between the peak power of the secondary pulse during $\langle \mathrm{OFF} \rangle$ state (biased at $0.9J_{\mathrm{th}}$) to the steady state power during $\langle \mathrm{ON} \rangle$ state (bias current is set to maintain constant steady-state output power), and the radiation loss variation is defined as the peak-to-peak difference between the radiation losses during $\langle \mathrm{ON} \rangle$ and $\langle \mathrm{OFF} \rangle$ state. In Fig. 10, it is noted that variation in s has a higher impact on the radiation loss and $\langle \mathrm{OFF/ON} \rangle$ ratio than that of d_2. This is because s is set to achieve resonance (high radiation loss) in the ARROW design, and hence any offset from this designated value will result in rapid deviation from the targeted radiation loss characteristics. However, if $s(d_2)$ is within an uncertainty of ± 0.01 μm (± 0.1 μm), the corresponding variation of $\langle \mathrm{OFF/ON} \rangle$ ratio is $\sim 0.05\%$, which is still acceptable.

E. Influence of Thermal Lensing Effects

The presence of thermal lensing effects will reduce the influence of carrier-induced index change, which in turn affects the design's capability to suppress the excitation of secondary pulsation. In addition, the increased modal confinement due to thermal lensing effects can also lead to multimode operation. Therefore, it is necessary to consider the influence of thermal lensing effects on the transient response of ARROW VCSELs in order to access the feasibility of the proposed design. Since the thermal time constant is of the order of μs, which is much longer than that of carrier lifetime ($\sim$ns), ΔT_r can be approximated as time-independent. As a result, the influence of thermal lensing effects on the transient response of ARROW VCSELs can be calculated by adding the steady-state heat-induced index variation at threshold to the built-in index profile of the ARROW waveguide.

For direct-modulated VCSEL under uncooled operation (i.e., without proper optimization of heatsink), the maximum rise of temperature $\Delta T_{\max} (= \Delta T_r|_{r=0})$ can be greater than 40 K, whereas in temperature-regulated condition, only a small rise in $\Delta T_{\max}$ (<10 K) is expected. To investigate the influence of thermal lensing effects, Fig. 11(a) plots the $\langle \mathrm{OFF/ON} \rangle$ ratio versus $\Delta T_{\max}$ and the insert shows the dependence of radiation loss on $\Delta T_{\max}$. The corresponding transverse temperature rise ΔT_r is also plotted in Fig. 11(b). Simulation results show that if $\Delta T_{\max}$ is less than 10 K, the ARROW VCSEL structure discussed in Section III-C operates under single-mode regime, and an $\langle \mathrm{OFF/ON} \rangle$ ratio lesser than 4% is easily attainable (see Fig. 11). For $\Delta T_{\max} > 10$ K, the structure will operate in multimode regime. This is in contrast to structure discussed in Section III-B, where mere inclusion of a small temperature rise inevitably leads to multimode operation. This shows that by operating the VCSEL under temperature regulated condition, designing ARROW close to resonance has the advantage of sustaining single-mode operation and ensuring a small $\langle \mathrm{OFF/ON} \rangle$ ratio.

$$\begin{bmatrix} \psi_i \\ \frac{\partial \psi_i}{\partial r} \end{bmatrix} = \begin{bmatrix} H_v^{(1)}(\beta_i r) & H_v^{(2)}(\beta_i r) \\ \frac{1}{2}\beta_i \left\{ H_{v-1}^{(1)}(\beta_i r) - H_{v+1}^{(1)}(\beta_i r) \right\} & \frac{1}{2}\beta_i \left\{ H_{v-1}^{(2)}(\beta_i r) - H_{v+1}^{(2)}(\beta_i r) \right\} \end{bmatrix} \begin{bmatrix} E_i^+ \\ E_i^- \end{bmatrix} \tag{A1}$$

IV. Summary and Conclusion

For ARROW VCSELs under current modulation, it is found that the radiation losses of the transverse-leaky mode varies during the $\langle \mathrm{ON} \rangle$ and $\langle \mathrm{OFF} \rangle$ states. During the $\langle \mathrm{ON} \rangle$ state, stimulated recombination causes depletion of carrier concentration within the core region. As a result, the magnitude of carrier-induced refractive-index depression is reduced, causing the radiation loss to decrease. During $\langle \mathrm{OFF} \rangle$ state, carrier-induced refractive-index depression shifts the transverse-leaky mode away from antiresonance condition of ARROW, resulting in an increase in radiation loss. It is noted that this variation in radiation loss can be used to prevent the net modal gain of the transverse-leaky mode from reacquiring threshold after turn-off, hence eliminating secondary pulsation during the turn-off transient. In order to make use of the variation of radiation losses in VCSELs, the ARROW dimension is selected close to resonance. During the turn-off transient of the VCSELs, the transverse-leaky mode temporarily satisfies resonance condition, resulting in a steep increment in radiation loss. This counters the effect of gain rebounce due to the refilling of SHB under the influence of carrier diffusion. Subsequent analysis shows that the presence of thermal lensing effects affects the resonant conditions of the ARROW. Therefore, secondary pulsation can only be suppressed effectively in ARROW VCSELs if the influence of thermal lensing effects is minimized.

In conclusion, the transient response of ARROW VCSELs has been investigated systematically. Simulations have addressed the unique radiation-loss-variation characteristics of current-modulated ARROW structure, elucidating its potential as a design parameter to realize single-mode lasers with high extinction ratio (low $\langle \mathrm{OFF}/\mathrm{ON} \rangle$ ratio). Investigations have shown that carrier-induced index-depression has significant influence on transient response of radiation losses of the transverse-leaky modes, allowing ARROW design to be optimized for the suppression of secondary pulsation. However, the inclusion of thermal lensing effects revealed the need for proper thermal management scheme for the proposed design to be feasible. Calculation shows that under temperature regulated operation, the design is robust against a weak influence of thermal lensing effects (i.e., $\Delta T_{\max} < 10$ K).

Appendix

In the analysis of the multilayered waveguide, boundary condition requires continuity of field profile $(\psi, \partial\psi/\partial r)$ across every interface. Using Hankel's function to describe the radial field profile, the matrix expression for the field and the corresponding derivative along the radial direction in the ith layer is given by (A1), shown at the top of the page [8].

Field profiles in adjacent layer can be related using a transfer matrix by rearranging (A1) and applying the boundary condition. The overall transfer matrix for the ARROW waveguide in Fig. 1 can then be written as

$$\left. \begin{bmatrix} \psi_1 \\ \frac{\partial \psi_1}{\partial r} \end{bmatrix} \right|_{r=0} = \prod_{i=1}^{3} \mathrm{TM}_i \left. \begin{bmatrix} \psi_4 \\ \frac{\partial \psi_4}{\partial r} \end{bmatrix} \right|_{r=r_4}. \tag{A2}$$

Applying axis-symmetric boundary condition on the left-hand side and radiation-mode boundary condition on the right-hand side of (A2), the eigenequation for the optical modes can be reduced to

$$\eta(n_{\mathrm{eff}}) = \mathrm{tm}_{21} + j\beta_4 \mathrm{tm}_{22} = 0 \tag{A3}$$

where tm_{21} and tm_{22} are the elements of the overall transfer matrix. (A3) can be solved numerically by varying the complex effective index n_{eff}. Propagation constant $(\beta_i = 2\pi\sqrt{n_i^2 - n_{\mathrm{eff}}^2}/\lambda)$ and radiation loss $(\alpha = 2\mathrm{Im}\{n_{\mathrm{eff}}\}/k_0)$ can then be obtained. Radiation loss can be computed as a function of time by discretizing the ARROW waveguide and solving (A3) at a small time step together with the numerical integration of the rate equations.

References

[1] A. Valle, J. Sarma, and K. A. Shore, "Secondary pulsations driven by spatial hole burning in modulated vertical-cavity surface-emitting laser diodes," *J. Opt. Soc. Amer. B*, vol. 12, no. 9, pp. 1741–1746, 1995.

[2] A. Valle and L. Pesquera, "Turn-off transients in current-modulated multitransverse-mode vertical-cavity surface-emitting lasers," *Appl. Phys. Lett.*, vol. 79, no. 24, pp. 3914–3916, 2001.

[3] J. J. Morikuni, P. V. Mena, A. V. Harton, K. W. Wyatt, and S. M. Kang, "Spatially independent VCSEL models for the simulation of diffusive turn-off transients," *J. Lightw. Technol.*, vol. 17, no. 1, pp. 95–101, Jan. 1999.

[4] J. Tatum, D. Smith, J. Guenter, and R. Johnson, "High speed characteristics of VCSELs," *Proc. SPIE*, vol. 3004, pp. 151–159, 1997.

[5] D. Zhou and L. J. Mawst, "High-power single-mode antiresonant reflecting optical waveguide-type vertical-cavity surface-emitting lasers," *IEEE J. Quantum Electron.*, vol. 38, no. 12, pp. 1599–1606, Dec. 2002.

[6] L. J. Mawst, D. Botez, R. F. Nabiev, and C. Zmudzinski, "Above-threshold behavior of high-power, single-mode antiresonant reflecting optical waveguide diode lasers," *Appl. Phys. Lett.*, vol. 66, no. 1, pp. 7–9, Jan. 1995.

[7] S. F. Yu, "Polarization selection in birefringent antiresonant reflecting optical waveguide-type vertical cavity surface emitting lasers," *IEEE. J. Quantum Electron.*, vol. 39, no. 11, pp. 1362–1371, Nov. 2003.

[8] C. W. Tee, C. C. Tan, and S. F. Yu, "Design of antiresonant reflecting optical waveguide-type vertical cavity surface emitting lasers using transfer matrix method," *IEEE Photon. Technol. Lett.*, vol. 15, no. 9, pp. 1231–1233, Sep. 2003.

[9] N. K. Dutta, "Analysis of current spreading, carrier diffusion, and transverse mode guiding in surface emitting lasers," *J. Appl. Phys.*, vol. 68, pp. 1961–1963, 1990.

[10] M. A. Duguay, Y. Kokubun, T. L. Koch, and L. Pfeiffer, "Antiresonant reflecting optical waveguides in SiO_2-Si multilayer structures," *Appl. Phys. Lett.*, vol. 49, no. 1, pp. 13–15, Jul. 1986.

C. W. Tee (S'04) received the B.Eng. degree in electrical and electronic engineering from Nanyang Technological University, Singapore, in 2003. He is currently working toward the Ph.D. degree at the Center for Photonic Systems, University of Cambridge, U.K.

His research interest includes semiconductor microring devices, high-brightness laser diodes and the modal characteristics of vertical-cavity surface-emitting lasers.

S. F. Yu (M'03–SM'03) received the B.Eng. degree from London University, University College, London, U.K., in 1990 and the Ph.D. degree from Cambridge University, Robinson College, Cambridge, U.K., in 1993.

Currently, he is an Associate Professor in the School of Electrical and Electronic Engineering, Nanyang Technological University, Singapore. His main research interest includes the fundamental study, design, and optimization of semiconductor lasers including distributed feedback lasers and vertical-cavity surface-emitting lasers. Recently, he has led to the design and fabrication of zinc oxide thin-film lasers emitted at ultraviolet wavelength. He has published over 110 international technical papers including invited conference and journal papers, two book chapters, and one book *Analysis and Design of Vertical Cavity Surface Emitting Lasers* (New York: Wiley, 2003).

Dr. Yu was one of the Guest Editors of the IEEE JOURNAL OF SELECTED TOPICS IN QUANTUM ELECTRONICS in the area of "Optoelectronics Device Simulation" on the May–June 2003 issue. He was on the executive committee of the seminar and meeting committee of the SPIE Hong Kong Chapter from 1996 to 2000. He was the Committee Member of the IEEE/LEOS Conference *Numerical Simulation of Optoelectronic Devices* held in August 2004. He is also the Program Cochair of the Symposum *N:ZnO and Related Materials, 3rd International Conference on Materials for Advanced Technologies* to be held in Singapore 2005.

R. V. Penty (M'00) recevied the B.Eng. degree in engineering and electrical sciences and the Ph.D. degree for research into nonlinear optical fiber devices from the University of Cambridge, U.K., in 1986 and 1990, respectively.

He was then as Science and Engineering Research Council (SERC IT) Research Fellow at the University of Cambridge until taking up a lectureship in physics at the University of Bath, Bath, U.K., in 1990. In 1996,he moved to the University of Bristol, Bristol, U.K., as a Lecturer in Electrical and Electronic Engineering and, subsequently, as a Professor of Photonics. In 2001, he moved to the University of Cambridge Engineering Department where he was also elected to a fellowship of Sidney Sussex College, Cambridge, in 2002. His research interests include optical data communications, magentomotive force (MMF) systems (digital and analog), high-speed optical communications systems, wavelength conversion and wavelength-division multiplexing networks, optical amplifiers, optical nonlinearities for switching applications, and high-power semiconductor lasers. He has been an author of more than 250 refereed journal and conference papers.

I. H. White (S'82–M'83–SM'00) received the B.Eng. degree in engineering and electrical sciences and the Ph.D. degree for research into multicontact semiconductor lasers from the University of Cambridge, Cambridge, U.K., in 1980 and 1984, respectively.

In 1990, he joined the University of Bath, Bath, U.K., as a Professor of Physics and then moved to the University of Bristol, Bristol, U.K., as a Professor of Optical Communications Systems. He became Van Eck Professor of Engineering with the University of Cambridge in October 2001. His current research interests are in the area of high-speed communication systems, local-area networks using optical links, vertical-cavity surface-emitting laser diodes, high-power short-pulse laser diodes, and multiwavelength communication sources and systems. He has published more than 350 journal and conference papers.